RESEARCH ARTICLE

ICY MOONS

Endogenous CO_2 ice mixture on the surface of Europa and no detection of plume activity

G. L. Villanueva[1]*, H. B. Hammel[2], S. N. Milam[1], S. Faggi[1,3], V. Kofman[1,3], L. Roth[4], K. P. Hand[5], L. Paganini[6], J. Stansberry[7], J. Spencer[8], S. Protopapa[8], G. Strazzulla[9], G. Cruz-Mermy[10], C. R. Glein[11], R. Cartwright[12], G. Liuzzi[13]

Jupiter's moon Europa has a subsurface ocean beneath an icy crust. Conditions within the ocean are unknown, and it is unclear whether it is connected to the surface. We observed Europa with the James Webb Space Telescope (JWST) to search for active release of material by probing its surface and atmosphere. A search for plumes yielded no detection of water, carbon monoxide, methanol, ethane, or methane fluorescence emissions. Four spectral features of carbon dioxide (CO_2) ice were detected; their spectral shapes and distribution across Europa's surface indicate that the CO_2 is mixed with other compounds and concentrated in Tara Regio. The $^{13}CO_2$ absorption is consistent with an isotopic ratio of $^{12}C/^{13}C = 83 \pm 19$. We interpret these observations as indicating that carbon is sourced from within Europa.

Jupiter's moon Europa is thought to host a subsurface ocean beneath an icy surface crust, which has a thickness estimated to be between 23 and 47 km (*1*). Spacecraft measurements have shown that Europa has an induced magnetic field, which has been interpreted as the result of a deep, salty ocean (*2*, *3*). Smaller liquid-water bodies might also be present within the ice shell (*4*). Europa's surface is one of the youngest in the Solar System, with the near absence of impact craters indicating an age in the range of 40 million to 90 million years (*5*). The extensive resurfacing is probably due to tidal heating sustained by orbital resonance—which could power cryovolcanism (*6*) (the eruption of water and volatiles through an ice crust at freezing temperatures)—and the upwelling of material to form ice domes (*7*). These processes would provide pathways for subsurface materials to reach the surface, where they could be observed.

Surface materials could be either endogenous (from within Europa) or exogenous (delivered by impacts or from Jupiter's magnetosphere); distinguishing between these possibilities is required to infer properties of the subsurface ocean (*8*). Europa's surface composition is dominated by water ice (*9*), with a complex mixture of other compounds, including salts (e.g., NaCl, hydrated sulfates) (*10*, *11*), and carbon- and sulfur-bearing molecular species (*12*–*14*). The diversity of observed species leads to uncertainty about the endogenous or exogenous nature of material on Europa's surface.

Searches for plume activity

A possible indication of endogenic material on Europa would be plumes: ejections of large amounts of material through cracks in the ice opened by the strong tidal forces. Evidence for plumes has been reported from ultraviolet observations of auroral emission lines of hydrogen and oxygen in the southern hemisphere, which were interpreted as the result of localized plumes containing up to 1×10^{32} molecules of H_2O (*15*). Such plume activity has not been confirmed by subsequent observations despite several attempts. Magnetic-field and plasma-wave observations from a close spacecraft flyby of Europa were interpreted as being caused by a plume (*16*). Transit observations of the Europa limb have also been interpreted as localized excess emission (*17*), or alternatively as statistical noise, not plume activity (*18*). Another study identified one tentative detection (at the 3σ level) of water-vapor plume activity within an otherwise quiescent period (*19*).

To search for active sources on Europa, we probed its atmosphere and surface using JWST (*20*), performing imaging with the Near-Infrared Camera (NIRCam) and spectroscopy in the 2.4- to 5.2-μm spectral range (Fig. 1) with the Near-Infrared Spectrograph (NIRSpec) at a resolving power of ~2700. The observations were carried out on 23 November 2022 to sample Europa's leading hemisphere (*21*). Searching for plume activity was done by probing the narrow molecular infrared features fluorescing in sunlight. We targeted the strong fundamentals bands of H_2O at 2.7 μm; CH_4, C_2H_6, and CH_3OH in the C–H stretch region (near 3.3 μm); and CO at 4.7 μm. We extracted an integrated spectrum across a 1.3–arc sec–diameter region centered on Europa (500 km beyond its radius), sampling the extended region beyond the moon's 1–arc sec diameter. We then removed solar and ice absorption features and compared the resulting residual spectra (fig. S1) with line-by-line fluorescence models by performing retrievals (*21*). We assumed an excitation rotational temperature of 25 K in the models, which is similar to the value measured in the plume of Enceladus (*22*).

None of the targeted molecules were detected in the Europa spectrum, and the resulting 3σ upper limits, in units of 10^{30} molecules, are <35 for H_2O, <18 for CH_4, <18 for C_2H_6, <93 for CH_3OH, and <14 for CO. Assuming an outgassing velocity of 583 m s^{-1} (*19*) and isotropic outflow, the upper limit of water (<35×10^{30} H_2O molecules) corresponds to a water-vapor plume activity of <1×10^{28} molecule s^{-1} (<300 kg s^{-1}). This upper limit for water is a factor of two lower than the previous tentative detection in the leading hemisphere [$(70 \pm 22) \times 10^{30}$ H_2O molecules (*19*)], a factor of four lower than that inferred from auroral ultraviolet emission lines on the anti-Jovian hemisphere [$(130 \pm 30) \times 10^{30}$ H_2O molecules (*15*)], and a factor of five lower than the median value [180×10^{30} H_2O molecules] reported for plumes at the trailing hemisphere (*17*). The JWST observations of the leading hemisphere set a limit on sustained water-plume activity on Europa; if any plume activity occurs on Europa today, it must be localized and weak (*16*), infrequent and inactive during our observations, or devoid of the volatile gases that we searched for.

CO_2 detection and isotope ratio

An alternative way to probe for endogenic sources on Europa is to search for recently deposited material on its surface. The NIRCam images (Fig. 2A), obtained by combining the observations with filters F140M [1.331 to 1.479 μm] and F212N [2.109 to 2.134 μm], show enhanced brightness in Tara Regio (10°S, 75°W), which is an area of chaos terrain, and also on the anti-Jovian side of Europa (180°W). The chaos terrain is an area of irregular groups of large blocks, which are thought to be related to an active geological process. Using the contemporaneously collected NIRSpec spectra of the leading hemisphere, we searched for evidence of CO, CH_4, or CH_3OH ices, but did not detect them. It has been suggested that CO_2 ice on Europa is concentrated on the anti-Jovian and trailing sides of its surface (*12*); however, the absorption bands were only marginally resolved in earlier data (*23*). Many nonwater ice bands

[1]NASA Goddard Space Flight Center, Greenbelt, MD 20771, USA. [2]Association of Universities for Research in Astronomy, Washington, DC 20004, USA. [3]American University, Washington, DC 20016, USA. [4]Royal Institute of Technology, Stockholm 104 50, Sweden. [5]Jet Propulsion Laboratory, Pasadena, CA 91109, USA. [6]NASA Headquarters, Washington, DC 20546, USA. [7]Space Telescope Science Institute, Baltimore, MD 21218, USA. [8]Southwest Research Institute, Boulder, CO 80302, USA. [9]Osservatorio Astrofisico di Catania, Istituto Nazionale di Astrofisica, 95123 Catania, Italy. [10]Universite Paris-Sarclay, 91190 Gif-sur-Yvette, France. [11]Southwest Research Institute, San Antonio, TX 78238, USA. [12]Carl Sagan Center for Research, Search for Extraterrestrial Intelligence Institute, Mountain View, CA 94043, USA. [13]Università degli Studi della Basilicata, 85100 Potenza, Italy.
*Corresponding author. Email: geronimo.villanueva@nasa.gov

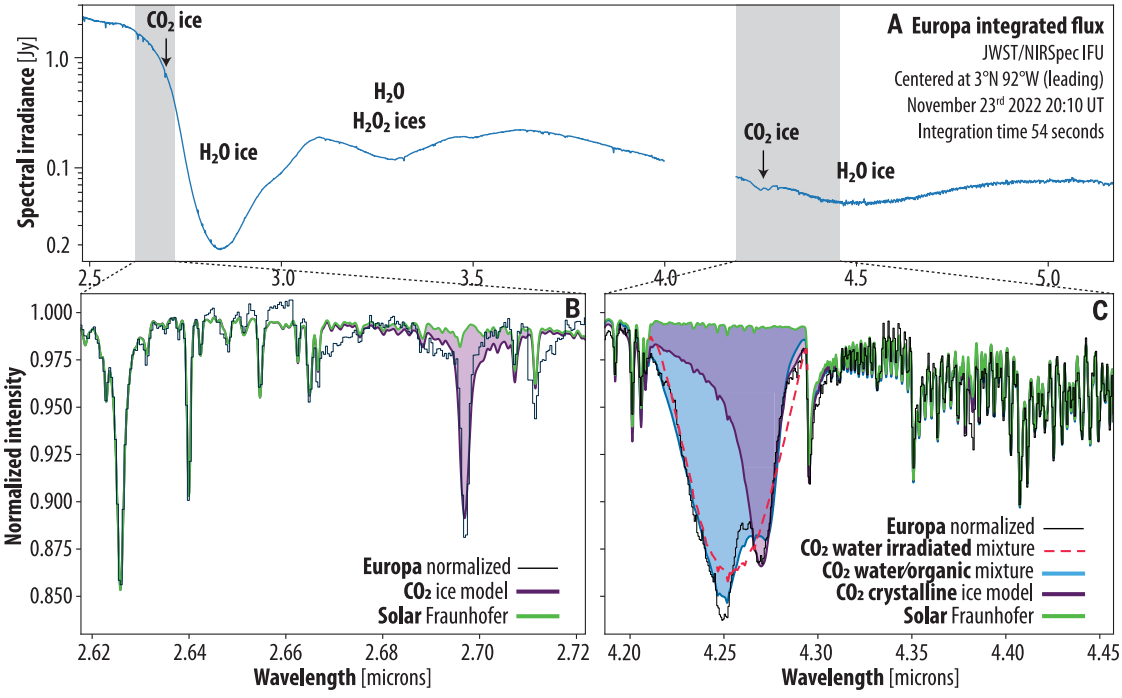

Fig. 1. Spectra of Europa's leading hemisphere acquired with JWST. (**A**) Spectrum from 2.5 to 5.2 μm (blue) expressed as spectral irradiance in janskys (Jy). Gray shaded regions indicate the ranges plotted in the other panels. Broad features due to H_2O and CO_2 ices are labeled. Narrower features are mostly Fraunhofer lines from sunlight reflected off Europa. (**B**) Zoomed spectrum (black histogram) around the band of crystalline CO_2 ice at 2.7 μm, normalized by the local continuum. The green line shows a solar spectrum used to identify the Fraunhofer lines. The dark purple line is a model of crystalline CO_2 ice; the light-purple shading indicates the integrated band strength used to produce the map in Fig. 2B. (**C**) Same as (B) except for the double-peaked CO_2 feature at 4.27 μm. The blue line is a model of a CO_2:H_2O:CH_3OH [1:0.8:0.9] mixture at 114 K. The shape of the observed spectrum is fitted with a combination of the blue and purple models. The peak position and width of the feature can alternatively be reproduced with a model (dashed red line) of carbonic acid synthesized in a CO_2:H_2O ice mixture (ratio 5:1) exposed to ionizing radiation.

have previously been mapped at hemisphere scales, including H_2O_2 at 3.5 μm (*24*), CO_2 at 4.3 μm (*12*), and SO_2 at 4.0 μm (*12*, *25*). If CO_2 is associated with endogenic landforms, then it would provide information on Europa's interior, such as the carbon content of the ocean. Theoretical models have predicted that the ocean contains dissolved CO_2 and other carbonate species (*26*), yet observations in the near infrared (1 to 2.5 μm) did not detect CO_2 (*27*) on Europa, so its presence and distribution remain unclear.

In the JWST data, we detected multiple features due to CO_2 ice on Europa: a narrow absorption band at 2.7 μm (Fig. 1B), a double-peaked absorption band at 4.25 and 4.27 μm (Fig. 1C), and an absorption due to the rarer isotopologue $^{13}CO_2$ at 4.38 μm (fig. S2C). $^{13}CO_2$ has previously been observed on two of Saturn's moons, Phoebe and Iapetus (*28*), but not on Europa. From the ratio of the $^{12}CO_2$ and $^{13}CO_2$ features, we estimate the carbon isotopic ratio $^{12}C/^{13}C = 83 \pm 19$ (1σ) (*21*). This value is consistent with the Earth inorganic standard [Vienna Peedee Belemnite (VPDB)], which has $^{12}C/^{13}C = 89$ (*29*). It is also consistent with measured values for Iapetus [$^{12}C/^{13}C = 83 \pm 8$ (*28*)] and with the range of $^{12}C/^{13}C$ ratios (between 83 and 85) measured from carbonate minerals in Ivuna-type carbonaceous chondrite meteorites and samples of the asteroid Ryugu (*30*). These values could reflect primordial (present in the protosolar nebula) CO_2, which could have been incorporated into Europa if it assembled from materials that formed at temperatures below ~80 K (*31*). Alternatively, the carbon in Europa's CO_2 could have been inherited from accreted primitive organic matter in the Solar System, which has $^{12}C/^{13}C = 90 \pm 1$ (*32*). The ratio of ^{12}C to ^{13}C is used as a biosignature on Earth (*33*), where localized carbon sources and reservoirs can have higher $^{12}C/^{13}C$ ratios (up to 104) as a result of biogenic processes (*29*). For C isotopes to serve as a biosignature on Europa, the isotopic fractionation between reduced carbon and CO_2 would need to be determined (*34*), which we cannot measure with these data, and therefore we cannot distinguish between abiotic or biogenic sources.

Nature and distribution of the CO_2 ice

The observed 4.25-μm absorption band due to $^{12}CO_2$ has a double-peaked structure, which differs from the single-peaked crystalline CO_2 ice (Fig. 1C). The synthetic spectrum of crystalline CO_2 ice in Fig. 1C was computed with the surface model of the Planetary Spectrum Generator (PSG) (*21*, *35*). The best match we found to this doubly peaked shape (Fig. 1C) was to a laboratory spectrum of a mixture of CO_2, H_2O, and CH_3OH in the ratio 1:0.8:0.9, respectively, measured at a temperature of 114 K (*36*). The temperature of this laboratory spectrum is within the range previously measured for different hemispheres of Europa (90 to 130 K) (*37*). This could indicate that CO_2 is stored in a water- and organic-rich matrix on Europa, yet we did not detect any bands in our spectra that were due to CH_3OH ice or other organic molecules. We regard methanol as a proxy for the effect of any organics on the band position of CO_2, and several other effects could also produce shifts in the CO_2 fundamental band (*21*, *38*). A blue-shifted CO_2 peak has previously been observed on Ganymede and Callisto (*39*, *40*) but did not show the same double-peak signature as we observe on Europa, perhaps because of differing spectral resolutions. The closest match to the CO_2 band detected on Callisto and Ganymede was a laboratory spectrum of carbonic acid (H_2CO_3) synthesized in a CO_2:H_2O ice mixture (in the ratio 5:1), then exposed to ionizing radiation in the form of 5-keV electrons (*41*). Similar laboratory irradiation experiments have been reported for Europa-like conditions (*42*). Figure 1C shows a synthetic spectrum based on the carbonic acid experiment (*41*), which reproduces the width and location of the band but not its double peak.

To test a possible matrix for the observed CO_2, we measured spectra of oceanic salt evaporite with a thin CO_2 ice film deposited onto the salts at different temperatures while being irradiated (*21*). In the experiments, the feature at 4.25 μm appeared after irradiation of the salts, whereas the feature at 4.27 μm was present in freshly deposited CO_2 (fig. S2C). We therefore interpret the 4.25-μm band as likely indicating CO_2 that was either adsorbed onto salts or captured within them.

We searched for heterogeneities in the CO_2 ice abundance and its structure by mapping

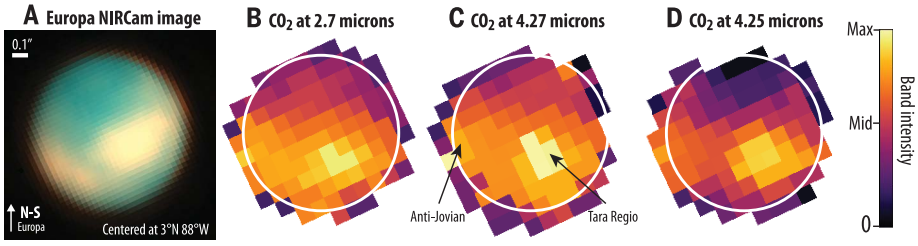

Fig. 2. Distribution of CO_2 on Europa. (**A**) A false-color image of Europa as it appeared during the JWST observations (*21*). The image is oversampled at 0.031 arc sec per pixel; the diffraction-limited resolution is ~0.08 arc sec at these wavelengths. (**B**) Distribution of the band intensity of the CO_2 2.7-μm feature, determined by fitting a model of CO_2 crystalline ice to the spectrum at each location. The white circle indicates the size of Europa in (A). (**C** and **D**) The 4.25- and 4.27-μm double-peaked feature was modeled as a combination of two components: CO_2 crystalline ice [band intensity shown in (C)] and CO_2 noncrystalline ice [band intensity shown in (D)]. (B), (C), and (D) share the same color bar but with different maximum/middle values of 0.70/0.35, 4.20/2.10, and 7.10/3.55 nm, respectively.

the strengths of the three $^{12}CO_2$ peaks across the observed hemisphere of Europa (Fig. 2); the $^{13}CO_2$ feature is too weak for mapping. For the mapping process and at each spatial point, we fitted a model of CO_2 crystalline ice for the 2.7-μm feature, whereas we modeled the 4.25- and 4.27-μm double-peaked feature as a combination of two components: CO_2 crystalline ice (using the model described above) and a CO_2 excess. The CO_2 excess model was constructed by subtracting the synthetic spectra of the mixture of CO_2, H_2O, and organic molecules from the crystalline CO_2 spectrum (Fig. 1C).

All three bands are strongest in the chaos terrain of Tara Regio, and the 2.7- and 4.27-μm CO_2 bands have similar distributions (Fig. 2). The 4.25-μm band has a larger dynamic range, with almost no detection in the northern regions and a lower abundance between Tara Regio and the anti-Jovian regions (Fig. 2D). The most abundant surface CO_2 appears to be in Tara Regio, potentially indicating that this geologically distinct region is associated with an endogenous source of CO_2. The distribution of the 4.25-μm CO_2 band is similar to that noted in previous observations of irradiated NaCl on Europa (*11*), whereas the 2.7-μm and 4.27-μm bands are distributed more broadly across Europa's surface. This is consistent with our interpretation (see above) that the 4.25-μm feature is due to CO_2 mixed with salts or produced through irradiation of carbonate salts.

An endogenous source of CO_2

CO_2 has been observed on a wide variety of Solar System objects and can have either native (endogenous) or nonnative (exogenous) origins. The localized CO_2 that we observe on Europa could be related to a disrupted surface, with a difference in the surface grain sizes affecting the strength of the CO_2 absorption across the surface (*43*). Exogenous explanations for the observed CO_2 on Europa are possible, but an exogenous source would likely produce a more global distribution, not the observed local concentration that is associated with salts (which are presumably endogenous). CO_2 ice is also localized on Enceladus, where it is known to be endogenous (*44*). Exogenous interplanetary dust grains might deliver carbonaceous material to Europa's icy surface, which could then yield CO_2 through radiolysis (*42*), but no silicate features indicative of such exogenous material have been reported for Europa (*25*). Given the CO_2 association with NaCl, and our laboratory results (*21*), we conclude that the most likely origin of the observed CO_2 is endogenous, at least within Tara Regio.

We consider several possible endogenous sources of CO_2. One possibility is that aqueous solutions rich in CO_2 are present in the subsurface. Such solutions could be present if a long-lived reservoir, such as Europa's ocean, has a low-enough pH (*26*), or if fluids migrating through Europa's ice shell incorporate CO_2 derived from destabilized dry ice or CO_2 clathrate hydrate (*45*).

A second potential source of CO_2 could be carbonate-bearing fluids (e.g., $NaHCO_3$ or Na_2CO_3 dissolved in water). Enceladus has a carbonate-rich ocean that degases CO_2 (*46*); some of that degassed CO_2 freezes out on the surface (*47*). An analogous process could occur on Europa. Alternatively, endogenous carbonates could react with acid compounds (e.g., H_2SO_4) at or near the surface to produce CO_2, or extruded brines [if they contain (bi)carbonate salts] could produce CO_2 during radiation processing (*48*).

A third possibility is that the carbon in the CO_2 might have been from organic compounds that were originally dissolved or suspended in a subsurface liquid-water reservoir, which were later converted to CO_2. CO_2 might be generated by irradiation on the surface, when material sourced from Europa's interior, rich in carbonate salts and/or organics mixed with H_2O, is bombarded by charged particles trapped in Jupiter's magnetosphere (*49*). A similar process has been proposed to form hydrogen peroxide (H_2O_2) from H_2O ice; H_2O_2 has previously been observed to be enriched at low latitudes across Europa's leading and anti-Jovian quadrants, including within the boundaries of Tara Regio (*50*). Because the surface environment of Europa is strongly oxidized, CO_2 would be produced by radiation-driven oxidation of reduced carbon species (organics) on Europa's surface; the lack of detectable CO could be an indication of that process (*49*).

Regardless of the specific source species of CO_2, we regard the presence of CO_2 in a region with previous indications of subsurface liquid water as evidence of carbon availability in Europa's interior.

REFERENCES AND NOTES

1. S. M. Howell, *Planet. Sci. J.* **2**, 129 (2021).
2. M. G. Kivelson *et al.*, *Science* **289**, 1340–1343 (2000).
3. N. Schilling, F. M. Neubauer, J. Saur, *Icarus* **192**, 41–55 (2007).
4. B. E. Schmidt, D. D. Blankenship, G. W. Patterson, P. M. Schenk, *Nature* **479**, 502–505 (2011).
5. P. M. Schenk, C. R. Chapman, K. Zahnle, J. M. Moore, in Cambridge Planetary Science series, vol. 1, *Jupiter: The Planet, Satellites and Magnetosphere*, F. Bagenal, T. E. Dowling, W. B. McKinnon, Eds. (Cambridge Univ. Press, 2004), pp. 427–456.
6. S. A. Fagents, *J. Geophys. Res.* **108**, 5139 (2003).
7. R. T. Pappalardo *et al.*, *Nature* **391**, 365–368 (1998).
8. K. P. Hand, C. F. Chyba, J. C. Priscu, R. W. Carlson, K. H. Nealson, in *Europa*, R. T. Pappalardo, W. B. McKinnon, K. Khurana, Eds. (Univ. of Arizona Press, 2009), pp. 589–629.
9. G. P. Kuiper, *Astron. J.* **62**, 245 (1957).
10. M. E. Brown, K. P. Hand, *Astron. J.* **145**, 110 (2013).
11. S. K. Trumbo, M. E. Brown, K. P. Hand, *Sci. Adv.* **5**, eaaw7123 (2019).
12. G. B. Hansen, T. B. McCord, *Geophys. Res. Lett.* **35**, L01202 (2008).
13. N. Ligier, F. Poulet, J. Carter, R. Brunetto, F. Gourgeot, *Astron. J.* **151**, 163 (2016).
14. T. B. McCord *et al.*, *J. Geophys. Res.* **103**, 8603–8626 (1998).
15. L. Roth *et al.*, *Science* **343**, 171–174 (2014).
16. X. Jia, M. G. Kivelson, K. K. Khurana, W. S. Kurth, *Nat. Astron.* **2**, 459–464 (2018).
17. W. B. Sparks *et al.*, *Astrophys. J.* **829**, 121 (2016).
18. G. Giono *et al.*, *Astron. J.* **159**, 155 (2020).
19. L. Paganini *et al.*, *Nat. Astron.* **4**, 266–272 (2020).
20. J. P. Gardner *et al.*, *Publ. Astron. Soc. Pac.* **135**, 068001 (2023).
21. Materials and methods are available as supplementary materials.
22. G. L. Villanueva *et al.*, *Nat. Astron.* 10.1038/s41550-023-02009-6 (2023).
23. R. W. Carlson, P. R. Weissman, W. D. Smythe, J. C. Mahoney, The NIMS Science and Engineering Teams, *Space Sci. Rev.* **60**, 457–502 (1992).
24. R. W. Carlson *et al.*, *Science* **283**, 2062–2064 (1999).
25. R. W. Carlson *et al.*, in *Europa*, R. T. Pappalardo, W. B. McKinnon, K. Khurana, Eds. (Univ. of Arizona Press, 2009), pp. 283–328.
26. M. Melwani Daswani, S. D. Vance, M. J. Mayne, C. R. Glein, *Geophys. Res. Lett.* **48**, e2021GL094143 (2021).
27. I. Mishra *et al.*, *Planet. Sci. J.* **2**, 183 (2021).
28. R. N. Clark, R. H. Brown, D. P. Cruikshank, G. A. Swayze, *Icarus* **321**, 791–802 (2019).
29. T. B. Coplen *et al.*, "Compilation of minimum and maximum isotope ratios of selected elements in naturally occurring terrestrial materials and reagents" (Water-Resources Investigations Report 01–4222, U.S. Geological Survey, 2001).
30. K. A. McCain *et al.*, *Nat. Astron.* **7**, 309–317 (2023).
31. O. Mousis, J. I. Lunine, A. Aguichine, *Astrophys. J. Lett.* **918**, L23 (2021).
32. C. M. O. Alexander, M. Fogel, H. Yabuta, G. D. Cody, *Geochim. Cosmochim. Acta* **71**, 4380–4403 (2007).
33. J. M. Hayes, K. H. Freeman, B. N. Popp, C. H. Hoham, *Org. Geochem.* **16**, 1115–1128 (1990).
34. M. van Zuilen, *Space Sci. Rev.* **135**, 221–232 (2008).
35. G. L. Villanueva *et al.*, *Fundamentals of the Planetary Spectrum Generator: 2022 Edition*. (NASA Goddard Space Flight Center, 2022).
36. P. Ehrenfreund *et al.*, *Astron. Astrophys.* **350**, 240–253 (1999).
37. J. A. Rathbun, N. J. Rodriguez, J. R. Spencer, *Icarus* **210**, 763–769 (2010).

38. D. P. Cruikshank *et al*., *Icarus* **206**, 561–572 (2010).
39. C. A. Hibbitts, T. B. McCord, G. B. Hansen, *J. Geophys. Res.* **105**, 22541–22557 (2000).
40. T. B. McCord *et al*., *Science* **278**, 271–275 (1997).
41. B. M. Jones, R. I. Kaiser, G. Strazzulla, *Astrophys. J.* **788**, 170 (2014).
42. K. P. Hand, R. W. Carlson, C. F. Chyba, *Astrobiology* **7**, 1006–1022 (2007).
43. R. N. Clark *et al*., *Icarus* **193**, 372–386 (2008).
44. J.-P. Combe *et al*., *Icarus* **317**, 491–508 (2019).
45. N. C. Shibley, G. Laughlin, *Planet. Sci. J.* **2**, 221 (2021).
46. C. R. Glein, J. H. Waite, *Geophys. Res. Lett.* **47**, e2019GL085885 (2020).
47. R. H. Brown *et al*., *Science* **311**, 1425–1428 (2006).
48. J. F. Cooper, R. E. Johnson, B. H. Mauk, H. B. Garrett, N. Gehrels, *Icarus* **149**, 133–159 (2001).
49. K. P. Hand, R. W. Carlson, *J. Geophys. Res.* **117**, E03008 (2012).
50. S. K. Trumbo, M. E. Brown, K. P. Hand, *Astron. J.* **158**, 127 (2019).

ACKNOWLEDGMENTS

This work is based on observations made with the NASA/ESA/CSA James Webb Space Telescope (JWST). The data were obtained from the Mikulski Archive for Space Telescopes (MAST) at the Space Telescope Science Institute, which is operated by the Association of Universities for Research in Astronomy under NASA contract NAS 5-03127 for JWST. We thank R. Carlson (1941 to 2022) for assisting in setting the guiding principles of the Europa observational program and in supporting the experimental framework at the Jet Propulsion Laboratory (JPL), California Institute of Technology, that we used in this work. **Funding:** G.L.V., S.F., and V.K. were supported by NASA's Goddard Astrobiology Program, Goddard's Fundamental Laboratory Research (FLaRe), and the Sellers Exoplanet Environments Collaboration (SEEC). S.N.M. and H.B.H. acknowledge support from NASA JWST Interdisciplinary Scientist grant no. 21-SMDSS21-0013. C.R.G. was supported by NASA through Europa Lander funding (award no. 80NSSC19K0611). L. R. acknowledges support from Swedish National Space Agency grant 2021-00153. K.P.H. acknowledges support from the NASA Astrobiology Program (award no. 80NSSC19K1427) and the Europa Lander Pre-Project, managed by the JPL under a contract with NASA. **Author contributions:** G.L.V., H.B.H., S.N.M., K.P.H., L.P., J.St., J.Sp., and G.S. designed and planned the observations. G.L.V., S.F., V.K., R.C., J.St., S.P., and G.L. analyzed the data, extracted calibrated spectra, produced the maps, and performed retrievals. C.R.G., L.R., and G.C.M. assisted with discussion and interpretation of the results. All authors contributed to the preparation, writing, and editing of the manuscript. **Competing interests:** The authors declare that they have no competing interests. **Data and materials availability:** The JWST data are available from MAST at https://mast.stsci.edu/portal/Mashup/Clients/Mast/Portal.html under proposal ID 1250. Our laboratory spectra are provided in data S1. Our data reduction scripts are provided in data S2.

SUPPLEMENTARY MATERIALS

science.org/doi/10.1126/science.adg4270
Materials and Methods
Figs. S1 and S2
References (*51*–*70*)
Data S1 and S2

Submitted 22 December 2022; accepted 22 August 2023
10.1126/science.adg4270